Supporting Information for:

Mn (II) mediated degradation of artemisinin based on Fe_3O_4@$MnSiO_3$-FA nanospheres for cancer therapy *in vivo*

Jian Chen,[#a] Weijie Zhang,[#b] Min Zhang,[b] Zhen Guo,[*c] Haibao Wang,[*d] Mengni He,[a] Pengping Xu,[a] Jiajia Zhou,[c] Zhenbang Liu,[c] Qianwang Chen[*a]

a. Hefei National Laboratory for Physical Sciences at Microscale, Department of Materials Science & Engineering, CAS High Magnetic Field Laboratory, University of Science and Technology of China, Hefei, 230026, China. E-mail: cqw@ustc.edu.cn; Fax & Fax: +86-551-63603005;

b. Hefei National Laboratory for Physical Sciences at Microscale and School of Life Sciences, University of Science and Technology of China, Hefei, 230027, China;

c. Anhui Key Laboratory for Cellular Dynamics and Chemical Biology, School of Life Sciences, University of Science and Technology of China, Hefei, 230027, China. E-mail: zhenguo@ustc.edu.cn;

d. Radiology Department of the First Affiliated Hospital of Anhui Medical University, Hefei, 230022, China. E-mail: whblqh@mail.ustc.edu.cn.

# These two authors contributed equally

* Corresponding author

Supporting Information Figures:

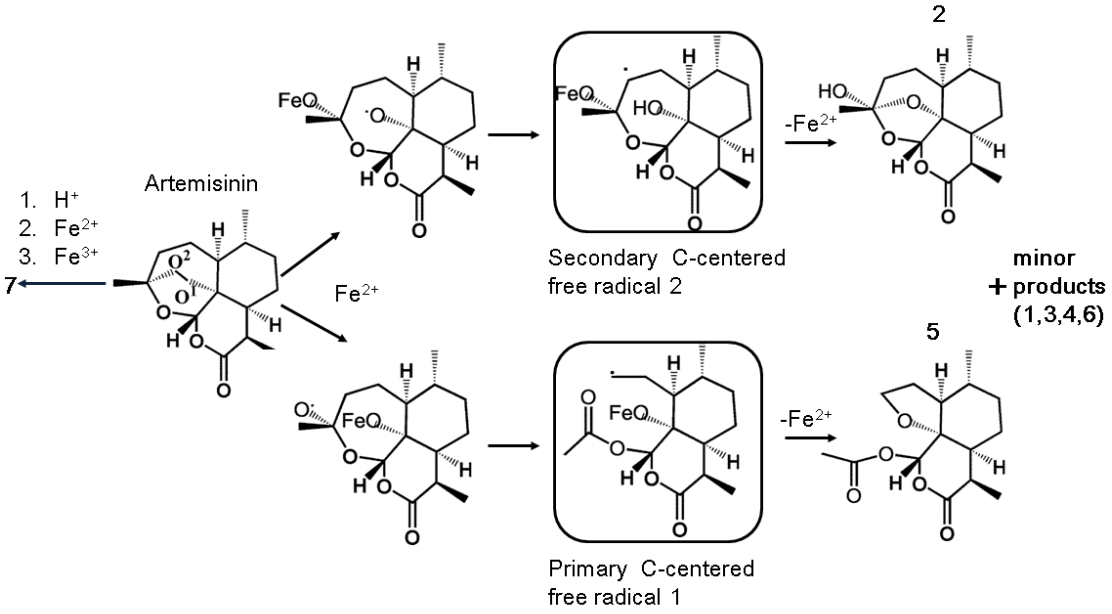

Figure S1. Iron mediated degradation mechanism for artemisinin. Products 1, 3, 4, and 6 are minor products of unknown structure observed by LCMS. Product 7 is an acid-mediated degradation product formed by reaction with either H^+, Fe^{3+}, or Fe^{2+}.

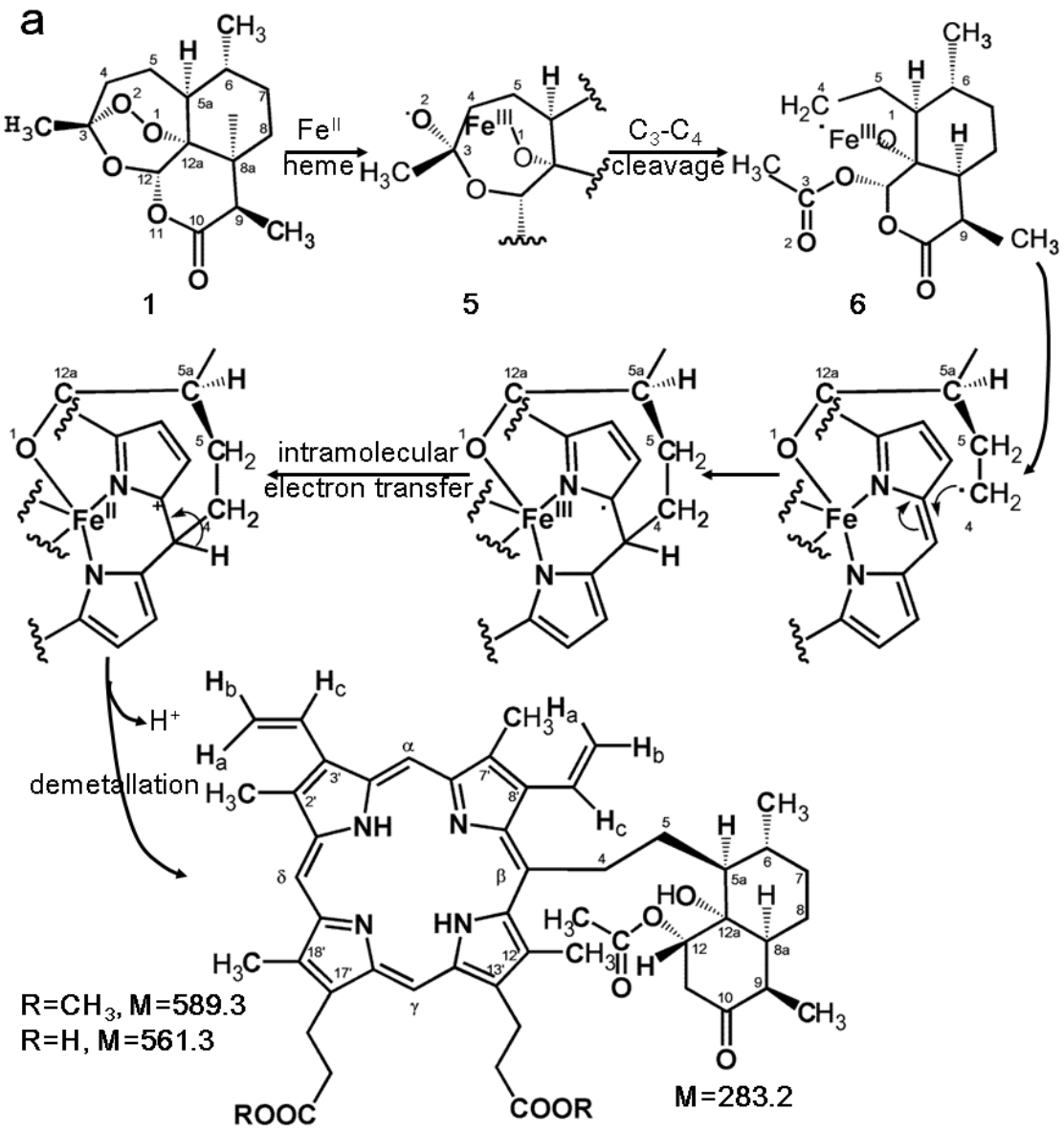

R=CH_3, H_2(PPIX-DME)-Art adducts	R=H, H_2(PPIX)-Art adducts
substitution at α position 7a	8a
substitution at β position 7b	8b
substitution at γ position 7c	8c
substitution at δ position 7d	8d
only 7b is depicted	only 8b is depicted
M=872.5	M=844.6

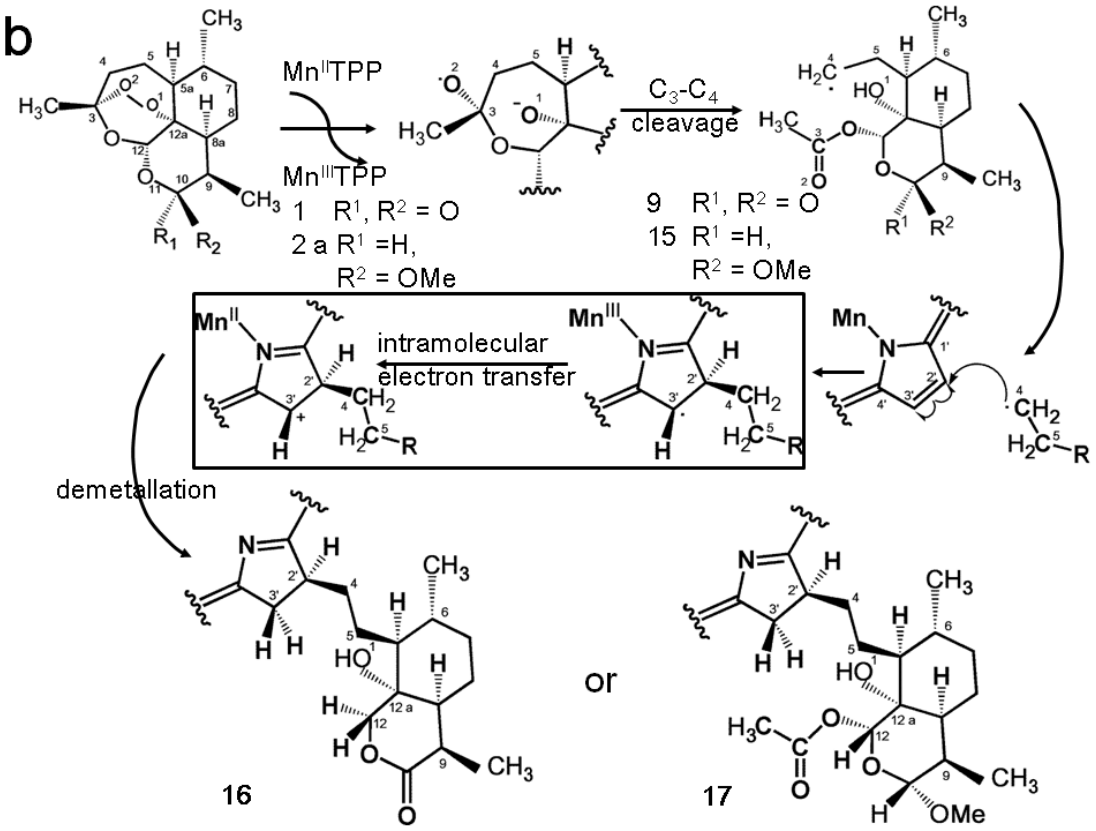

Figure S2. (a) Alkylation of iron(II)-heme or iron(II)/heme dimethylester by artemisinin, leading after demetallation to the covalent adducts 7a-d and 8a-d, respectively; (b) Mechanism of alkylation of the heme model $Mn^{II}TPP$ by artemisinin.

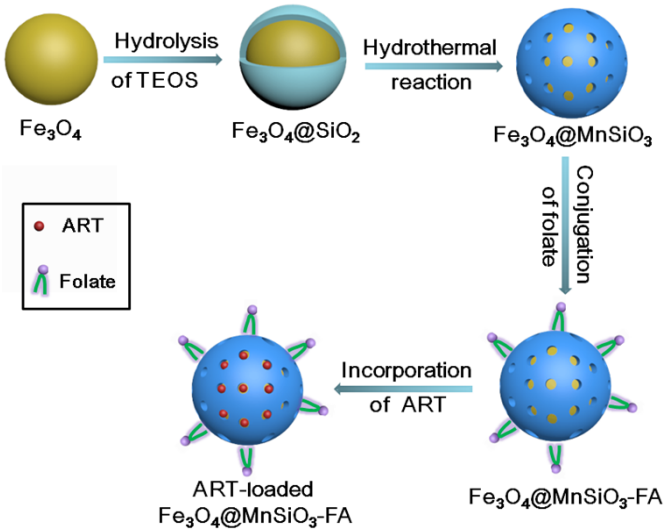

Figure S3. Schematic illustration of the synthesis of ART-loaded Fe_3O_4@$MnSiO_3$-FA nanospheres.

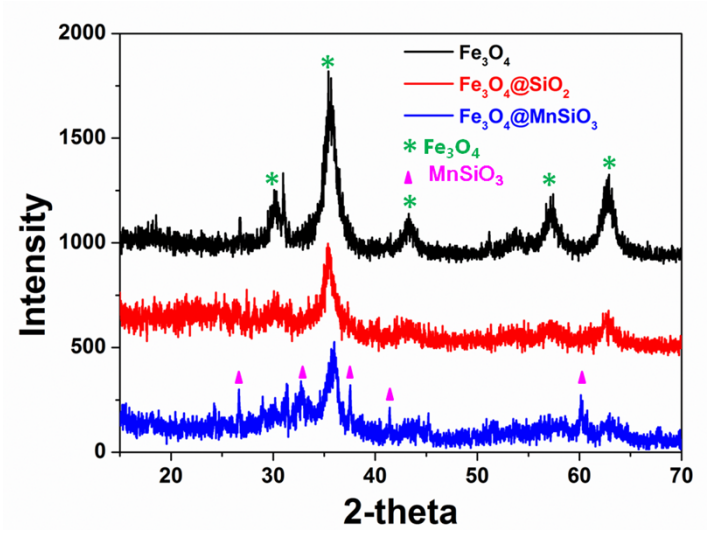

Figure S4. X-ray diffraction pattern for the products of Fe_3O_4, Fe_3O_4@SiO_2 and Fe_3O_4@$MnSiO_3$.

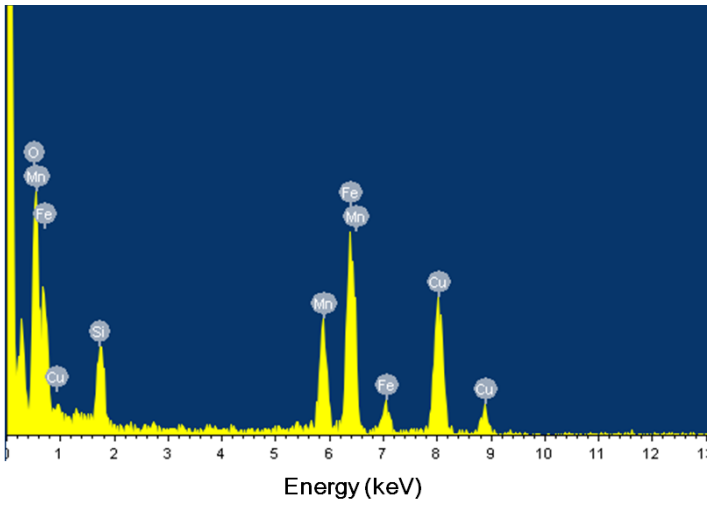

Figure S5. EDX spectrum of Fe_3O_4@$MnSiO_3$ nanospheres**.**

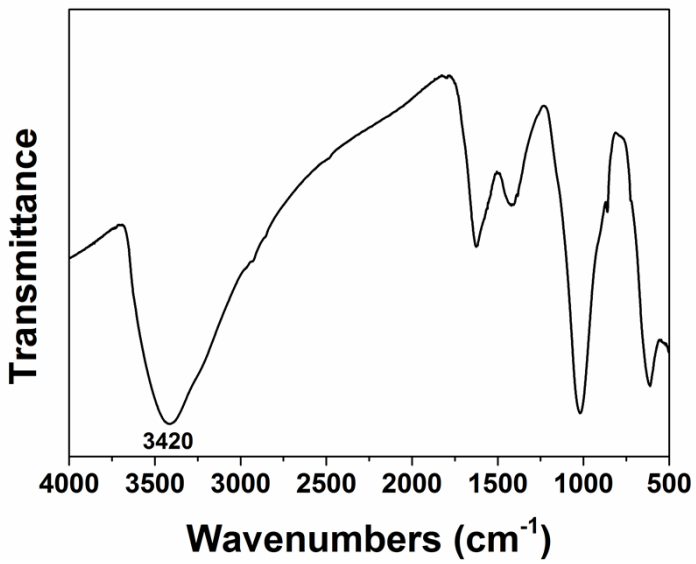

Figure S6. FT-IR spectrum of Fe_3O_4@$MnSiO_3$ nanospheres.

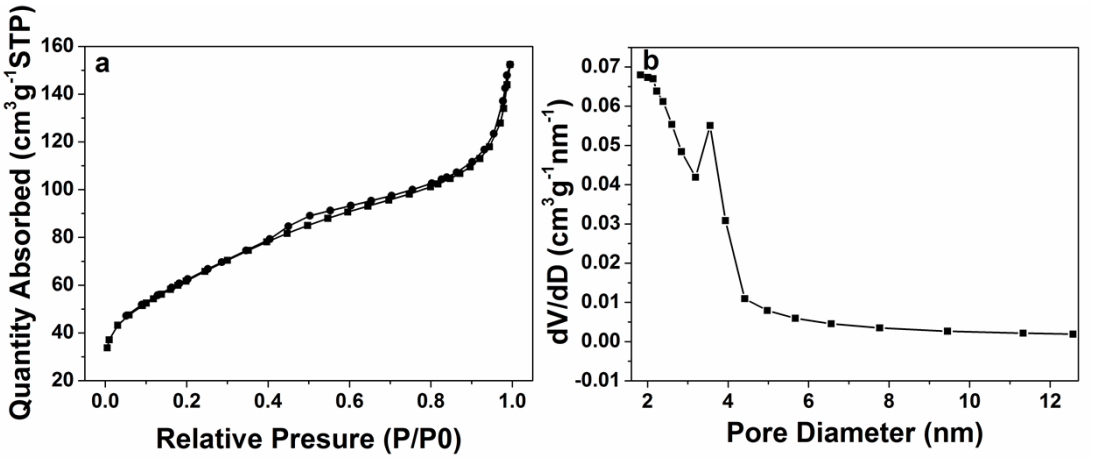

Figure S7. (a) N_2 adsorption and desorption isotherm and (b) BJH pore distribution of Fe_3O_4@$MnSiO_3$ nanospheres.

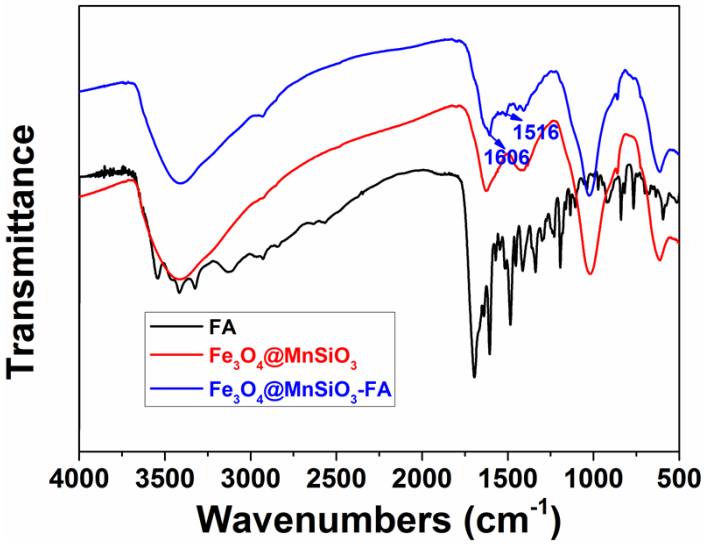

Figure S8. FT-IR spectra of FA, Fe_3O_4@$MnSiO_3$ nanopheres and Fe_3O_4@$MnSiO_3$-FA nanospheres.

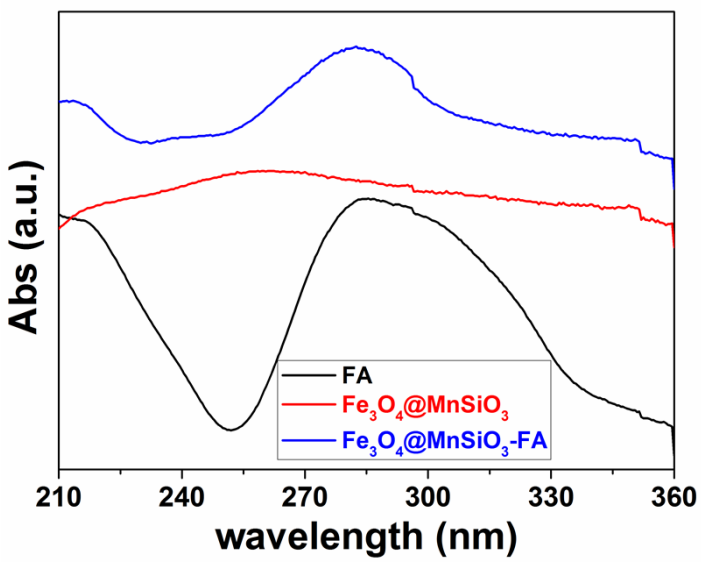

Figure S9. UV-vis spectra of FA, Fe_3O_4@$MSiO_3$ nanopheres and Fe_3O_4@$MnSiO_3$-FA nanospheres.

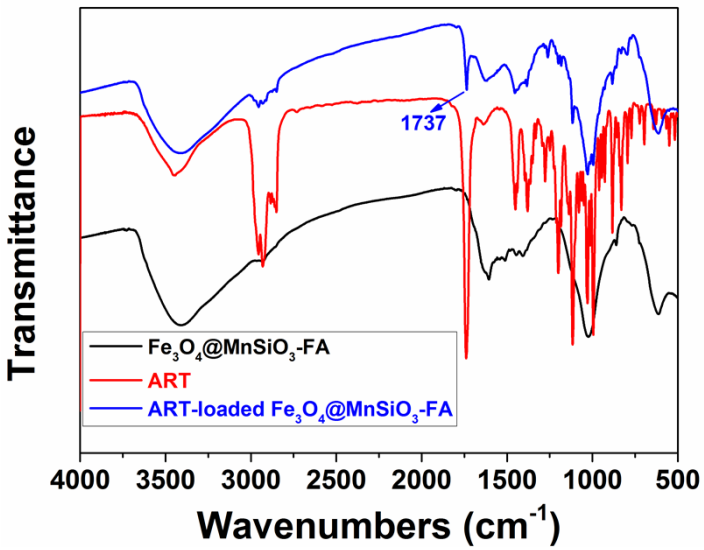

Figure S10. FT-IR spectra of standard ART, Fe_3O_4@$MnSiO_3$-FA nanopheres and ART-loaded Fe_3O_4@$MnSiO_3$-FA nanospheres.

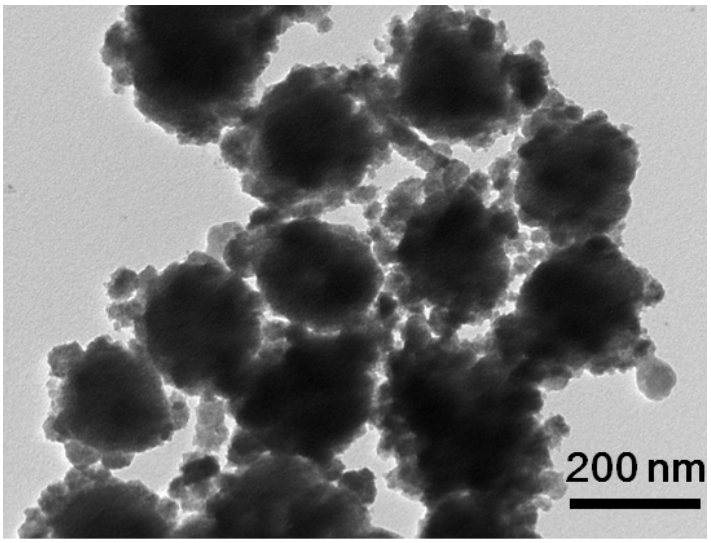

Figure S11. TEM images of Fe_3O_4@$MnSiO_3$ nanospheres kept in PBS with pH 5.5 for 24 h.

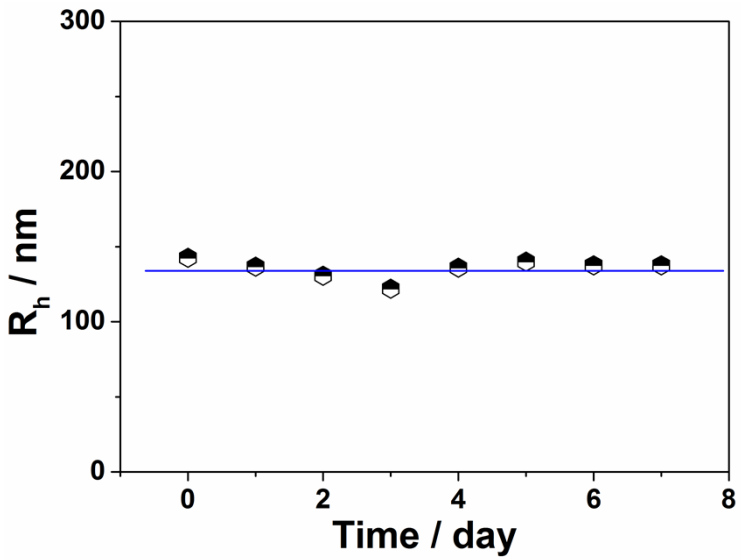

Figure S12. In vitro stability of ART-loaded Fe_3O_4@$MnSiO_3$-FA nanospheres. The size of the nanospheres in distilled water was measured by a commercial laser light scattering (LLS) spectrometer (ALV/DLS/SLS-5022 F).

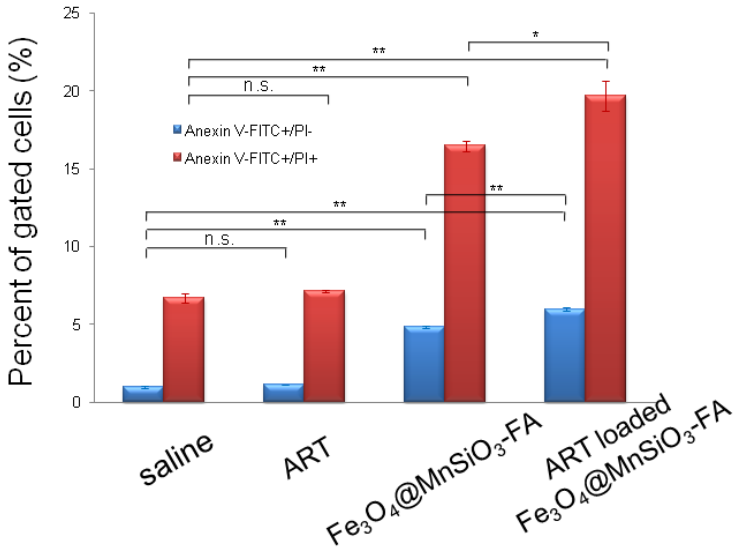

Figure S13. Parallel test results of flow cytometric detection in A549 cells treated with (a) saline, (b) ART, (c) Fe_3O_4@$MnSiO_3$-FA nanospheres and (d) ART-loaded Fe_3O_4@$MnSiO_3$-FA nanospheres at concentrations of ART 16.5 μg/mL or Fe_3O_4@$MnSiO_3$-FA nanospheres 75 μg/mL. n.s., not siginificant; *, $p<0.05$; **, $p<0.001$.

Supporting Information Table:

	pH 7.4	**pH 6.8**	**pH 5.5**
Released Fe^{2+} (%)	**0.033**	**0.084**	**0.12**
Released Mn^{2+} (%)	**0.92**	**3.53**	**12.59**

Table S1. Fe^{2+} or Mn^{2+} release from Fe_3O_4@$MnSiO_3$ nanospheres in PBS at different pHs (7.4, 6.8, 5.5).